

Contrib Mineral Petrol (2007) 154:717–730
DOI 10.1007/s00410-007-0222-8

ORIGINAL PAPER

Quantifying garnet-melt trace element partitioning using lattice-strain theory: new crystal-chemical and thermodynamic constraints

Wim van Westrenen · David S. Draper

Received: 16 August 2006 / Accepted: 17 May 2007 / Published online: 5 September 2007
© Springer-Verlag 2007

Abstract Many geochemical models of major igneous differentiation events on the Earth, the Moon, and Mars invoke the presence of garnet or its high-pressure majoritic equivalent as a residual phase, based on its ability to fractionate critical trace element pairs (Lu/Hf, U/Th, heavy REE/light REE). As a result, quantitative descriptions of mid-ocean ridge and hot spot magmatism, and lunar, martian, and terrestrial magma oceans require knowledge of garnet-melt partition coefficients over a wide range of conditions. In this contribution, we present new crystal-chemical and thermodynamic constraints on the partitioning of rare earth elements (REE), Y and Sc between garnet and anhydrous silicate melt as a function of pressure (P), temperature (T), and composition (X). Our approach is based on the interpretation of experimentally determined values of partition coefficients D using lattice-strain theory. In this and a companion paper (Draper and van Westrenen this issue) we derive new predictive equations for the ideal ionic radius of the dodecahedral garnet X-site, $r_0(3+)$, its apparent Young's modulus $E_X(3+)$, and the strain-free partition coefficient $D_0(3+)$ for a fictive REE element J of ionic radius $r_0(3+)$. The new calibrations remedy several shortcomings of earlier lattice-strain based attempts to

model garnet-melt partitioning. A hitherto irresolvable temperature effect on $r_0(3+)$ is identified, as is a pronounced decrease in $E_X(3+)$ as Al on the garnet Y site is progressively replaced by quadrivalent cations (Si, Ti) as pressure and garnet majorite content increase. $D_0(3+)$ can be linked to the free energy of fusion of a hypothetical rare-earth garnet component $\text{JFe}_2\text{Al}_3\text{Si}_2\text{O}_{12}$ through simple activity-composition relations. By combining the three lattice-strain parameter models, garnet-anhydrous melt and majorite-anhydrous melt D values for the REE, Y and Sc can be predicted from P , T , garnet major element composition, and melt iron content at pressures from 2.5–25 GPa and temperatures up to 2,573 K, covering virtually the entire P – T range over which igneous garnets are stable in solar system compositions. Standard deviations of the difference between predicted and observed $D_{\text{REE,Y,Sc}}$ range from 25% for Er to 70% for Ce, and are not correlated with trace element mass. The maximum error in D prediction ($n > 300$) is 218% for one measurement of D_{Dy} . This is remarkably low considering the total spread in D values of over four orders of magnitude.

Communicated by T. L. Grove.

W. van Westrenen (✉)
Faculty of Earth and Life Sciences,
Vrije Universiteit Amsterdam, De Boelelaan 1085,
1081 HV Amsterdam, The Netherlands
e-mail: wim.van.westrenen@falw.vu.nl

D. S. Draper
Institute of Meteoritics,
Department of Earth and Planetary Sciences,
University of New Mexico, Albuquerque,
NM 87131-1136, USA

Introduction

Trace elements are sensitive trackers of magmatic processes, due to their passive nature and widely varying physical and chemical properties (e.g., Goldschmidt 1937; Shaw 1953; Blundy and Wood 2003a). Quantitative models to constrain partial melting and crystallisation in the interiors of the Earth and other rocky planetary bodies (e.g., Neumann et al. 1954; Gast 1968; Shaw 1970; Allègre and Minster 1978; Zou and Reid 2001) all require mineral-melt partition coefficients D (where D is the concentration

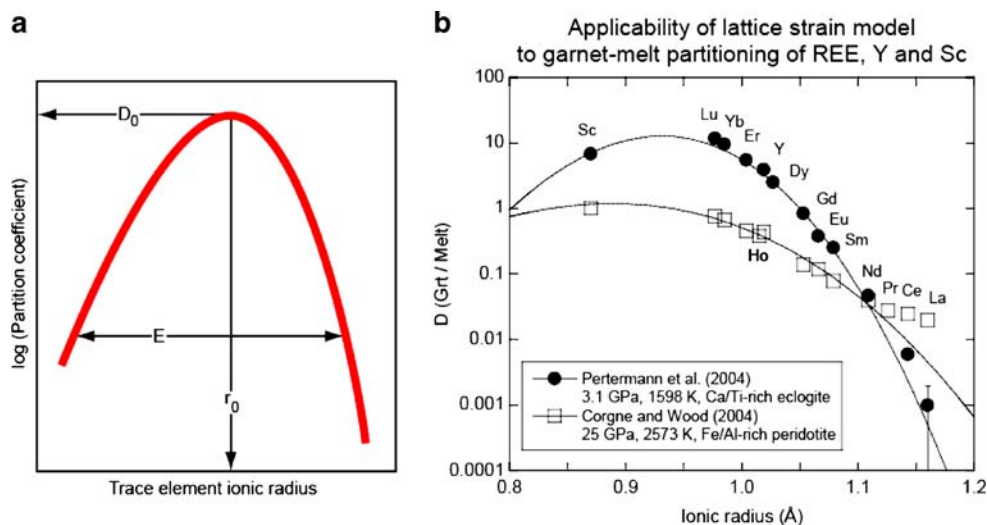
ratio between mineral and melt, following the terminology of Beattie et al. (1993) as input parameters. Although they are often assumed to be constant, D 's are thermodynamic variables, changing as a function of pressure, temperature, and composition (e.g., Hertogen and Gijbels 1976; Beattie 1994; Blundy and Wood 1994, 2003a, b; Wood and Blundy 2001, 2002; Gaetani 2004; Mysen 2004; Prowatke and Klemme 2005).

The crystal lattice-strain model (Blundy and Wood 1994, 2003a, b) provides a convenient framework for the development of models that quantify the extent of these D variations. This model builds upon the observation, first made by Onuma et al. (1968), that the logarithms of mineral-melt partition coefficients D_i for a series of trace elements i with charge $j+$, substituting onto a particular crystal lattice site, show a near-parabolic dependence on trace element radius r_i (Fig. 1a). This dependence can be related to the energetics of exchanging major and trace elements in both crystal and co-existing melt, if it is assumed that these energetics are dominated by the crystal lattice-strain energy (Nagasawa 1966; Brice 1975) required to accommodate a misfit trace element in a crystal lattice site.

The resulting lattice-strain model uses three parameters to describe D variations (Eq. 1, Fig. 1a): (1) The 'ideal radius' r_0 for a (fictive) element with charge $j+$ that does not strain the crystal lattice and hence has the largest mineral-melt D . (2) The maximum partition coefficient D_0 for this 'ideally sized' element. (3) The apparent Young's modulus E of the site, which is a measure of the resistance of the crystal lattice to the incorporation of elements with radii larger or smaller than the ideal radius r_0 .

$$D_i = D_0 \exp \left(\frac{-4\pi EN_A \left(\frac{r_0}{2} (r_i - r_0)^2 + \frac{1}{3} (r_i - r_0)^3 \right)}{RT} \right) \quad (1)$$

Fig. 1 **a** Sketch showing parameters of the lattice-strain model (Eq. 1) in relation to the observed near-parabolic dependence of $\log(D)$ on trace element radius. **b** Examples of measured garnet-melt partition coefficients (symbols, data from Corgne and Wood (2003) and Pertermann et al. (2004) for REE, Sc, and Y showing parabolic behaviour. Curves are fits of Eq. 1 to the data



where R is gas constant, T in Kelvin, and N_A Avogadro's number.

Here, we present a lattice-strain based thermodynamic model for the partitioning of REE, Y and Sc between garnet, majorite and anhydrous silicate melt applicable at pressures from 2.5 to 25 GPa. Many geochemical models of major igneous differentiation events on the Earth, Mars, and the Moon invoke the presence of garnet or majorite (a mineral with the garnet structure, but containing significantly higher Si and lower Al concentrations) as a residual phase (e.g., Kato et al. 1988; Drake et al. 1993; Neal 2001; Borg and Draper 2003; Corgne and Wood 2004; Walter et al. 2004), based on the ability of these minerals to fractionate critical trace element pairs (e.g., Lu/Hf, U/Th, heavy REE/light REE). Quantitative descriptions of mid-ocean ridge and hot spot magmatism, and lunar, martian, and terrestrial magma ocean evolution thus require knowledge of garnet-melt partition coefficients over a wide range of conditions (e.g., Salters and Longhi 1999; van Westrenen et al. 1999, 2000a; Klemme et al. 2002; Salters et al. 2002; Bennett et al. 2004; Pertermann et al. 2004; Corgne and Wood 2004; Draper et al. 2003, 2006; Dwarzski et al. 2006).

A sketch of the cubic garnet crystal structure (e.g., Gibbs and Smith 1965; Ungaretti et al. 1995) is shown in Fig. 2. The structure consists of a 3D network of interconnected polyhedra including X-site dodecahedra, Y-site octahedra, and Z-site tetrahedra, leading to the general formula $X_3Y_2Z_3O_{12}$. Majorite-free aluminosilicate garnets of interest to Earth Science have the general formula $X_3Al_2Si_3O_{12}$, where the major element composition of the X-site is dominated by a mixture of divalent Ca, Mg, Mn, and Fe. Both garnet-melt partitioning studies and EXAFS measurements show that the REE replace these divalent X-site cations (e.g., van Westrenen et al. 1999; Quartieri et al. 1999a, b, 2002, 2004). As pressure increases, excess

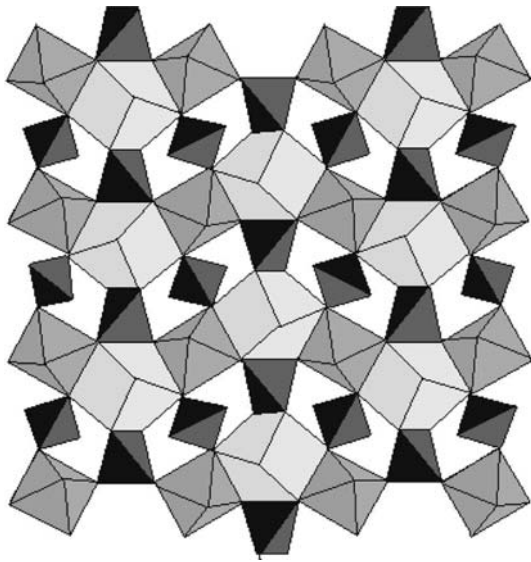


Fig. 2 Two-dimensional projection of the build-up of the garnet and majorite structures, after Merli et al. (1995). Alternating isolated tetrahedra (black, enclosing the Z site) and octahedra (dark grey, enclosing the Y site) form a 3D corner-sharing network, with the resulting cavities forming dodecahedra (light grey, enclosing the X site)

Si is incorporated into the garnet structure by replacing Al in the Y-site. Garnets with >3 Si and <2 Al atoms per formula unit (apfu) are classified as ‘majoritic garnet’ or ‘majorite’.

The large extent of the P – T stability field of garnet and majorite, combined with the substantial variations in published garnet-anhydrous melt D values for the REE of up to four orders of magnitude, make this a highly suitable test case for the limits of application of lattice-strain models. Previous attempts at formulating predictive garnet-melt REE partitioning models (van Westrenen et al. 2001; Wood and Blundy 2002) failed to predict correctly both majorite-melt D ’s (Draper et al. 2003, 2006; Dwarzski et al. 2006) and garnet-melt D ’s at low temperatures (e.g., Klemme et al. 2002; Bennett et al. 2004; Pertermann et al. 2004). As shown in this and a companion paper (Draper and van Westrenen this issue), experimental data published over the past 6 years allow lattice-strain based constraints on D variations to be improved significantly.

This manuscript presents the data base used for the development of the predictive models, and describes the new crystal-chemical and thermodynamic constraints on r_0 , E and D_0 variations derived from it. In the Draper and van Westrenen (this issue) companion paper a complementary approach is taken to predicting variations in the three lattice-strain model parameters. Detailed statistical evaluations of correlations between intensive and extensive

controlling parameters are presented, allowing for the incorporation of terms that reflect a contribution from melt composition in predicting variations in D_0 . The resulting D_0 model performs as well as the thermodynamic model presented in this paper. By combining the new lattice-strain parameter models, garnet-melt and majorite-melt D values for the REE, Y and Sc can be predicted in anhydrous systems at pressures from 2.5 to 25 GPa and temperatures up to 2,573 K, covering virtually the entire P – T range over which igneous garnets are stable in solar system compositions.

Methods

A total of 57 published experimental garnet-anhydrous melt and majorite-anhydrous melt partitioning data sets (Table 1) were considered for the construction of predictive models, representing a threefold increase compared to previous work (van Westrenen et al. 2001; Wood and Blundy 2002). The P – T field covered by the data is shown in Fig. 3. Pressures in the experiments ranged from 2.4 to 25 GPa, and temperatures covered a range from 1,603 to 2,573 K. The pioneering majorite-melt partitioning studies of Kato et al. (1988), Ohtani et al. (1989), Yurimoto and Ohtani (1992), and Moriyama et al. (1992) were not incorporated to exclude the possibility of partitioning data artefacts, related to the short run durations and small grain sizes employed in these studies (see discussion in Corgne and Wood 2004), although as detailed in Draper and van Westrenen (this issue), statistical analyses do not identify results of these studies as major outliers.

Three notable improvements in the input data set are: (1) Improved temperature coverage at a pressure of 3 ± 0.2 GPa. (2) Improved coverage at pressures exceeding 5 GPa. (3) Improved compositional coverage, including martian and terrestrial mantle compositions that produce garnets with significant majorite components (Draper et al. 2003, 2006; Walter et al. 2004; Corgne and Wood 2004), eclogitic bulk compositions (Klemme et al. 2002; Bennett et al. 2004), Ti-rich terrestrial compositions (Pertermann et al. 2004), and very Ti-rich compositions relevant to melting in the lunar mantle (Dwarzski et al. 2006).

Measured REE/Y/Sc D values for these experiments were fitted to Eq. 1 for each experiment, using a Levenberg–Marquardt-type weighted non-linear least-squares fitting routine (Press et al. 1992). Two representative sample data sets and corresponding best-fit curves are shown in Fig. 1b. Systematic trends in r_0 , E , and D_0 were linked quantitatively to variations in garnet/majorite crystal-chemical composition, melt composition, temperature, and pressure, to arrive at a predictive lattice-strain based partitioning model.

Table 1 Pressure–temperature conditions for anhydrous garnet–melt and majorite–melt partitioning experiments considered in this study

References	Experiment	<i>P</i> (GPa)	<i>T</i> (K)	References	Experiment	<i>P</i> (GPa)	<i>T</i> (K)
Salter et al. (2002)	TM1295-10	2.4	1,738	van Westrenen et al. (1999)	14	3.0	1,803
Hauri et al. (1994)		2.5	1,703	van Westrenen et al. (2000a)	18	3.0	1,811
Salter et al. (2002)	BK797-3	2.8	1,853	Withers (1997)	AOB1.08	3.0	1,743
Salter et al. (2002)	RD-893-6	2.8	1,858	Withers (1997)	AOB1.11	3.0	1,760
Salter et al. (2002)	MO1295-3	2.8	1,788	Pertermann et al. (2004)	MP236	3.1	1,598
Salter and Longhi (1999)	TM694-3	2.8	1,808	Salter et al. (2002)	RD1097-4	3.2	1,873
Salter and Longhi (1999)	TM694-6	2.8	1,820	Salter et al. (2002)	RD1097-5	3.2	1,883
Salter and Longhi (1999)	TM295-4	2.8	1,813	Salter et al. (2002)	RD1097-7	3.4	1,908
Salter and Longhi (1999)	MO895-1	2.8	1,823	Salter et al. (2002)	RD1097-8	3.4	1,933
Salter and Longhi (1999)	MO895-2	2.8	1,803	Draper et al. (2006)	A67	3.5	2,048
Salter and Longhi (1999)	MO895-3	2.8	1,773	Draper et al. (2006)	A138	4.0	1,873
Salter and Longhi (1999)	TM1295-2	2.8	1,788	Draper et al. (2006)	A140	4.5	1,873
Pertermann et al. (2004)	A343	2.9	1,663	Rocholl et al. (1996)	829	5.0	1,853
van Westrenen et al. (2000a)	16	2.9	1,813	Rocholl et al. (1996)	832	5.0	1,913
Bennett et al. (2004)	SB/4/2000	3.0	1,675	Draper et al. (2006)	A221	5.0	1,923
Bennett et al. (2004)	SB/8/2001	3.0	1,603	Draper et al. (2006)	A228	5.0	1,898
Johnson (1998)		3.0	1,703	Draper et al. (2003)	R223+R243	5.0	2,023
Klemme et al. (2002)	BS21	3.0	1,673	Dwarzski et al. (2006)	A85	5.5	1,923
Pertermann et al. (2004)	MP169	3.0	1,628	Dwarzski et al. (2006)	A161	5.5	1,943
Pertermann et al. (2004)	MP214	3.0	1,633	Dwarzski et al. (2006)	A119	6.3	1,973
Pertermann et al. (2004)	MP240	3.0	1,613	Dwarzski et al. (2006)	A103	7.0	1,923
Pertermann et al. (2004)	MP220	3.0	1,623	Draper et al. (2003)	R180+R252	7.0	2,133
Pertermann et al. (2004)	MP216	3.0	1,623	Draper et al. (2003)	R242+R236	7.0	2,048
Pertermann et al. (2004)	MP237	3.0	1,623	Draper et al. (2006)	A229	7.0	2,048
Pertermann et al. (2004)	MP254	3.0	1,623	Draper et al. (2003)	R244+R233	9.0	2,073
van Westrenen et al. (1999)	8	3.0	1,833	Walter et al. (2004)	62	23	2,573
van Westrenen et al. (1999)	11	3.0	1,838	Walter et al. (2004)	249	23.5	2,573
van Westrenen et al. (1999)	12	3.0	1,818	Corgne and Wood (2004)		25	2,573
van Westrenen et al. (1999)	13	3.0	1,803				

Results and discussion

A new model for r_0

Fitted values of r_0 vary from 0.88 to 0.99 Å. Experiments at constant pressure (3 ± 0.1 GPa) and temperature ($1,818 \pm 15$ K) and varying bulk composition previously showed that r_0 for the REE, Y and Sc is linked linearly to garnet X-site composition (van Westrenen et al. 1999, 2000a):

$$r_0 (\text{Å at 3 GPa, 1818 K}) = 0.9302 X_{\text{Py}} + 0.993 X_{\text{Gr}} + 0.916 X_{\text{Alm}} + 0.946 X_{\text{Spes}} + 1.05 (X_{\text{And}} + X_{\text{Uv}}), \quad (2)$$

where X is mole fraction, Py = pyrope ($\text{Mg}_3\text{Al}_2\text{Si}_3\text{O}_{12}$), Gr = grossular ($\text{Ca}_3\text{Al}_2\text{Si}_3\text{O}_{12}$), Alm = almandine ($\text{Fe}_3\text{Al}_2\text{Si}_3\text{O}_{12}$), Spes = spessartine ($\text{Mn}_3\text{Al}_2\text{Si}_3\text{O}_{12}$),

And = andradite ($\text{Ca}_3\text{Fe}_2\text{Si}_3\text{O}_{12}$), and Uv = uvarovite ($\text{Ca}_3\text{Cr}_2\text{Si}_3\text{O}_{12}$).

Based on observed variations in r_0 in a limited number of experiments performed at pressures between 2.5 and 5 GPa, the pressure dependence of r_0 was previously constrained to -0.005 Å/GPa (van Westrenen et al. 2000a). This pressure dependence leads to severe mismatches between observed and predicted r_0 at pressures near the upper pressure stability limit of majorite (>20 GPa). For example, the van Westrenen et al. (2000a, 2001) calibration predicts $r_0 = 0.82$ Å for the Corgne and Wood (2004) and Walter et al. (2004) experiments at 23–25 GPa, compared to the observed values that range from 0.88 to 0.91 Å.

In the new model, the measured pressure dependence of the dimensions of the large dodecahedral garnet X-site, on which the REE are known to reside (e.g., Quartieri et al. 1999a, b, 2002, 2004), is used as an independent means to

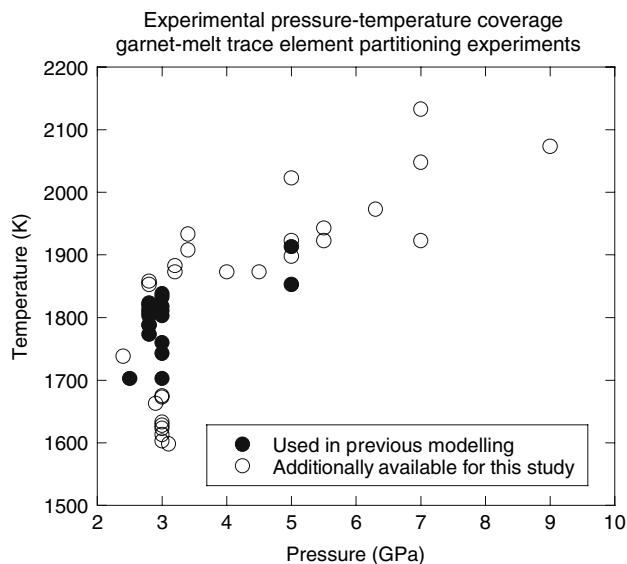


Fig. 3 Pressure–temperature conditions of experimental garnet–anhydrous melt partitioning data sets used in this study, compared to the earlier work of van Westrenen et al. (2001) and Wood and Blundy (2002). Not shown are three data sets at 23–25 GPa and 2,573 K (Walter et al. 2004; Corgne and Wood 2004), included in this study and absent from the 2001 and 2002 data bases

constrain the pressure dependence of r_0 . The decrease in average dodecahedral cation–oxygen distance $\langle X-O \rangle$ with increasing pressure was determined to high accuracy by Zhang et al. (1998) for end-member pyrope ($Mg_3Al_2Si_3O_{12}$) garnet (Fig. 4). These data were taken to be representative for the behaviour of r_0 in all garnet and majorite

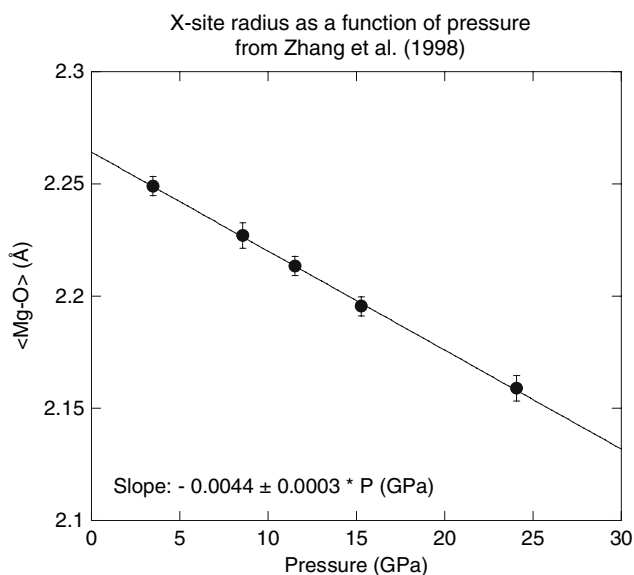


Fig. 4 Variation of average Mg–O distance in $Mg_3Al_2Si_3O_{12}$ pyrope, $\langle Mg-O \rangle$, as a function of pressure between 2.5 and 25 GPa, taken from single crystal X-ray diffraction refinements of Zhang et al. (1998)

compositions. As shown in Fig. 4, $\langle X-O \rangle$ varies linearly across the complete pressure range relevant to igneous garnet/majorite stability (i.e., between 2.5 and 25 GPa), leading to a predicted change in r_0 of $-0.0044 \pm 0.0003 \text{ \AA/GPa}$.

The preponderance of experiments at $3 \pm 0.1 \text{ GPa}$ (Table 1, Fig. 3) allows for the unambiguous identification of a clear temperature dependence of r_0 , with r_0 varying at a rate of $0.000058 \pm 0.000007 \text{ \AA/K}$ (Fig. 5). Although intuitively it seems reasonable to expect an increase in r_0 values with increasing temperature as crystal lattices expand, due to the small temperature ranges involved this effect could not be resolved previously in lattice-strain based REE mineral–melt partitioning models. The resulting predictive equation for r_0 incorporating both compositional, P , and T effects (with compositions given in terms of mole fractions of the garnet end-members, P in GPa, and T in Kelvin, and taking the values of 3 GPa and 1,818 K mentioned above as anchor points) is given below (Eq. 3):

$$r_0(\text{REE}, \text{\AA}) = 0.9302 X_{Py} + 0.993 X_{Gr} + 0.916 X_{Alm} + 0.946 X_{Spes} + 1.05 (X_{And} + X_{Uv}) - 0.0044(\pm 0.0003) (P - 3) + 0.000058(\pm 0.000007) (T - 1818). \quad (3)$$

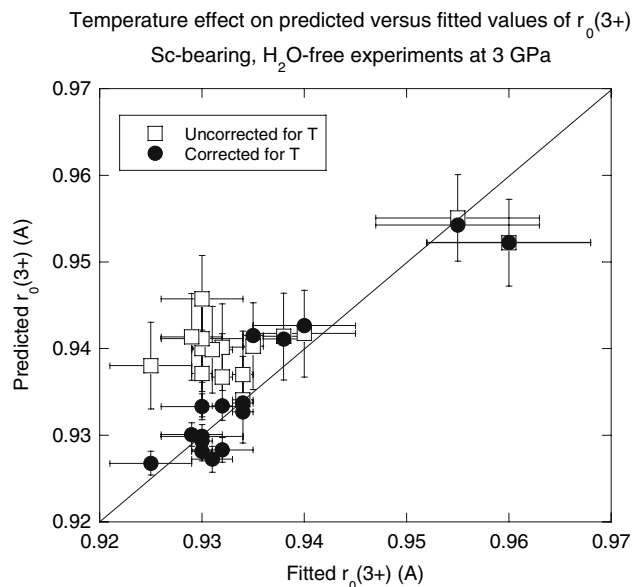


Fig. 5 Comparison between predicted and observed values of r_0 for REE partitioning between garnet and anhydrous silicate melt at 3 GPa (taken from references listed in Table 1). Open symbols depict predictions using the r_0 model of van Westrenen et al. (2000a, b) (Eq. 2), showing significant overestimation of r_0 at low values of fitted r_0 (coinciding with experiments performed at relatively low temperatures). Linear regression analysis leads to the identification of a significant temperature effect on r_0 . Incorporation of this effect into the predictive model for r_0 (filled symbols, obtained using Eq. 3) leads to significant reduction of the mismatch between observed and predicted values

For majoritic garnets, mole fractions to be used in Eq. 3 were calculated as follows: First, all Ca, Fe²⁺, Mn²⁺, Na and K was assigned to the large X site. Mg was then divided between the X-site (leading to a total of three cations per formula unit) and the Y site. The pyrope fraction X_{Py} was then calculated looking at the X-site composition only. We opted to assume only Mg entered the smaller majorite Y-site, because it is the smallest of the major 1+/2+ cations in majorite. Alternative site assignments (e.g., partially assigning Fe²⁺, Mn and Mg to the Y-site) would lead to a slightly different fit parameter for the temperature dependence in Eq. 3.

Equation 3 predicts r_0 for all 57 experimental data sets to within 0.017 Å (1σ), compared to 0.032 Å (1σ) achievable with van Westrenen et al. (2000a, 2001). The 2001 model performed increasingly badly as pressure increased towards the upper majorite stability limit of approximately 25 GPa in terrestrial mantle compositions (Walter et al. 2004; Corgne and Wood 2004). Crucially, the new model shows no correlation between absolute and relative values of r_0 misfit and experimental pressure.

Notably, this major improvement was achieved without introducing into Eq. 3 any explicit term dealing with variations in garnet octahedral Y site composition, related to the incorporation of excess Si (in the case of majorite-bearing garnets) or Ti (in the case of Ti-rich experiments). Ostensibly, within the accuracy required for interpreting element partitioning data, the effective radius r_0 of the large dodecahedral X site in garnet and majorite appears unaffected by changes in the compositions of the Y (and tetrahedral Z) sites. Neither increasing garnet Ti content (Bennett et al. 2004; Pertermann et al. 2004; Dwarzski et al. 2006), nor increasing majorite content with increasing pressure (Draper et al. 2003, 2006; Corgne and Wood 2004; Walter et al. 2004) affect r_0 for the REE. As discussed in the next section, this contrasts sharply with observed variations of the apparent Young's modulus E of the garnet X site, predictions of which do require explicit incorporation of the effect of the presence of Si and/or Ti on the garnet Y site.

A new model for E

The observed apparent Young's modulus E for trivalent trace elements entering the garnet X site is large, both in absolute terms, and in relative terms compared to E values for trivalent cations entering crystallographic sites in other important igneous minerals, such as the clinopyroxene M2 site (e.g., Wood and Blundy 1997). Fitted 3+ E values for the experiments listed in Table 1 range from 465 ± 40 GPa to 730 ± 32 GPa. These high values reflect the ability of garnet to fractionate heavy from light REE to a much larger extent than most other major rock-forming minerals,

leading to steep REE patterns in melts produced in the presence of residual garnet (the so-called 'garnet signature' identified in many terrestrial mantle melts, e.g., Salters and Hart 1989; Shen and Forsyth 1995; Hellebrand et al. 2002).

Blundy and Wood (1994) used an empirical relationship derived from a compilation of elastic property measurements of polyhedra in minerals (Hazen and Finger 1979) to link the Young's modulus of a polyhedron enclosing a crystal lattice site to the site effective radius r_0 and the charge Z_c of the cation occupying the site:

$$E \text{ (GPa)} = 1125(\pm 30) Z_c (1.38 + r_0 \text{ (\AA)})^{-3}. \quad (4)$$

The good agreement between apparent Young's moduli derived by fitting Eq. 1 to REE plagioclase-melt and clinopyroxene M2 site-melt partitioning data, and actual measurements of plagioclase and clinopyroxene polyhedral Young's moduli provided strong support in favour of using lattice-strain models to interpret partitioning data (Blundy and Wood 1994). However, although Eq. 4 holds well in these cases, it significantly underestimates the high fitted E values for 3+ elements entering the large site in garnets and majorites (van Westrenen et al. 2000a, b).

Young's moduli of garnet structures cover the range 245–275 GPa (depending on chemical composition), virtually identical to the range for reported majorite values (240–285 GPa) (Whitney et al. 2007; van Westrenen unpublished compilation). Corrected from the nominal charge of 2+ to a charge of 3+ using the Hazen and Finger (1979) formalism, this translates into 'expected' E values between 360 and 428 GPa. All apparent Young's moduli derived from garnet-melt and majorite-melt partitioning datasets lie significantly above this range. The discrepancy becomes even larger when considering that the Young's modulus of the garnet XO_8 polyhedron is lower than that of the garnet structure as a whole, as it is the most compressible polyhedron in the structure. For example, the measured Young's modulus of the MgO_8 in pyrope is 160 ± 1 GPa, compared to 257 ± 3 GPa for the bulk mineral (Zhang et al. 1998).

As noted previously (van Westrenen et al. 2000a, b), the Hazen and Finger relation (Eq. 4) therefore cannot be used as a predictive model for E . Garnets and majorites are not unique in this respect: even larger deviations have been reported for the clinopyroxene M1 site (Hill et al. 2000) and the Zr site in zircon (e.g., Hanchar and van Westrenen 2007). Van Westrenen et al. (2000b) extensively discussed possible reasons for the mismatch between apparent Young's modulus and 'true' modulus, and we refer the reader to that publication for more information.

van Westrenen et al. (2000a) took an alternative, empirical approach to predicting E . They found that, in

accordance with data compilations by Anderson (1972) for oxide, halide and sulphide compounds, a power law dependence of E on r_0 could reproduce observed E values:

$$E(\text{REE in garnet, GPa}) = 1.17 \times 10^{12} Z_c (1.38 + r_0(\text{REE in garnet, \AA}))^{-26.7} \quad (5)$$

Figure 6 shows how poorly Eq. 5 performs when applied to Si-rich (majorite-bearing) and Ti-rich experimental data. On average, Eq. 5 overestimates E values for all data obtained at $P > 5$ GPa by >300 GPa, far exceeding the average error on the fitted value of E in this pressure range (73 GPa). A fundamental shortcoming of Eq. 5 in light of majorite-melt partitioning data is that it predicts rapidly increasing E values as r_0 decreases (crosses in Fig. 6). All studies of majorite-melt and Ti-rich garnet-melt partitioning of REE listed in Table 1 (Draper et al. 2003, 2006; Corgne and Wood 2004; Walter et al. 2004; Dwarzski et al. 2006) agree that fitted E values for Si/Ti-rich garnets are *smaller* than E values for garnets without a majorite/Ti component, while at the same time fitted (and predicted) values of r_0 in majoritic garnets are smaller (squares in Fig. 6).

This observation is incompatible with any simple mineral-physics based theoretical model for the variation of Young's modulus with crystal lattice site dimension. Its origin may lie in the energetics of charge-balancing the incorporation of trivalent REE into the divalent X-site as mentioned above (e.g., van Westrenen 2000b; Dwarzski

et al. 2006), or possibly in anomalous behaviour of the compressibility of the majorite X-site compared to the X-site in non-majoritic garnet. In the absence of detailed models for the compressibility of the majoritic garnet X-site, we have opted for the new predictive E model to be empirical in nature. The new model was constructed through linear regression of observed E values against temperature, pressure, and an explicit measure of the extent of the majorite component (Eq. 6, with r_0 taken from Eq. 2, P in GPa, T in Kelvin, and $(\text{Al} + \text{Cr})_{\text{apfu}}$ the number of atoms per formula unit (12 oxygen) of Al and Cr in garnet):

$$E(\text{GPa}) = 2826(\pm 174)(1.38 + r_0)^{-3} + 12.4(\pm 1.3)P - 0.072(\pm 0.007)T + 237(\pm 8)(\text{Al} + \text{Cr})_{\text{apfu}} \quad (6)$$

The signs of the regressed temperature and pressure terms are physically realistic: minerals become more incompressible as P increases, leading to larger E , whereas they become more easily compressible as T increases, leading to smaller E . As the concentrations of 4+ cations on the garnet Y-site (Si and Ti) increase, $(\text{Al} + \text{Cr})_{\text{apfu}}$ decreases, leading to a decrease in E , as observed. Figure 6 shows how good the agreement is between fitted and predicted values of E , compared to previous model predictions (van Westrenen et al. 2001; Wood and Blundy 2002). Equation 6 predicts E for all experiments in Table 1 to within 78 GPa (1σ). This value is close to the average standard deviation for fitted values of E (52 GPa, 1σ), and constitutes a major improvement compared to the average standard deviation of 221 GPa (1σ) achievable with the old calibration.

A new model for D_0 : thermodynamic treatment

Governing equations

Previous studies have shown that D_0 values can be linked to the major element composition of both mineral and co-existing melt, pressure and temperature (e.g., Blundy and Wood 2003a). We quantified the dependence of D_0 on each of these variables using the thermodynamic approach pioneered by Blundy et al. (1995), as subsequently used for the prediction of clinopyroxene-melt and garnet-melt REE D 's (Wood and Blundy 1997, 2002; van Westrenen et al. 2001). For an extensive discussion of the philosophy behind this approach we refer the reader to van Westrenen et al. (2001).

The basis of a thermodynamic treatment of garnet-melt D_0 variations for the rare-earth elements is a fusion equilibrium for a fictive garnet component (defined in general terms as 'J-garnet' in the discussion below) that

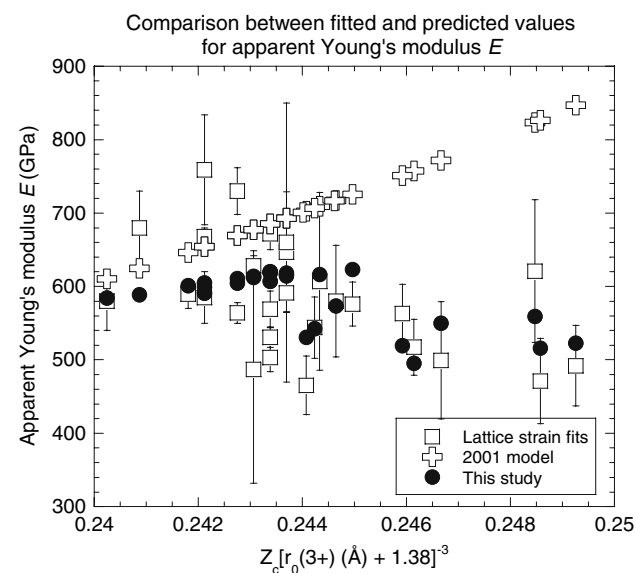


Fig. 6 Comparison between fitted values of apparent Young's modulus E (squares), predicted values from the 2001 model (crosses) and the new predictions using Eq. 4 from this study (circles). Error bars are 1σ

incorporates a hypothetical rare-earth element J^{3+} with ideal radius r_0 :

$$J\text{-garnet}(\text{garnet}) = J\text{-garnet}(\text{melt}). \quad (7)$$

Taking the standard states to be pure J-garnet solid and liquid at the P and T of interest, the standard state Gibbs free energy change ΔG_f^0 for this reaction at P and T is then given by

$$\begin{aligned} \Delta G_{f(P,T)}^0 &= \Delta H_{f(0.1,T_f)}^0 + \int_{T_f}^T \Delta C_P^0 dT \\ &\quad - T \left[\Delta S_{f(0.1,T_f)}^0 + \int_{T_f}^T \left(\frac{\Delta C_P^0}{T} \right) dT \right] + \int_{0.1\text{MPa}}^P \Delta V^0 dP \end{aligned} \quad (8)$$

where $\Delta H_{f(0.1,T_f)}^0$, ΔC_P^0 , $\Delta S_{f(0.1,T_f)}^0$, and ΔV^0 , denote differences in thermodynamic properties between pure J-garnet melt and crystal at 0.1 MPa and T_f (the hypothetical melting temperature of pure J-garnet at 0.1 MPa). Along the melting curve of pure J-garnet $\Delta G_f^0(P,T) = 0$, leading to

$$\begin{aligned} \Delta H_{f(0.1,T_f)}^0 - T \Delta S_{f(0.1,T_f)}^0 \\ = - \int_{T_f}^T \Delta C_P^0 dT + T \int_{T_f}^T \left(\frac{\Delta C_P^0}{T} \right) dT - \int_{0.1\text{MPa}}^P \Delta V^0 dP \end{aligned} \quad (9)$$

In natural systems where garnet and melt coexist, the compositions of crystals and melts are not equal to those of pure J-garnet. In this case, instead of being equal to zero, ΔG_f^0 in Eq. 8 will depend on the activities (a) of the J-garnet component in garnet and melt:

$$\Delta G_{f(P,T)}^0 = RT \ln \left(\frac{a_{J\text{-garnet}}^{\text{garnet}}}{a_{J\text{-garnet}}^{\text{melt}}} \right). \quad (10)$$

Equation 9 then becomes

$$\begin{aligned} \Delta H_{f(0.1,T_f)}^0 - T \Delta S_{f(0.1,T_f)}^0 &= - \int \Delta C_P^0 dT + T \int \left(\frac{\Delta C_P^0}{T} \right) dT \\ &\quad - \int \Delta V^0 dP + RT \ln \left(\frac{a_{J\text{-garnet}}^{\text{garnet}}}{a_{J\text{-garnet}}^{\text{melt}}} \right). \end{aligned} \quad (11)$$

Again, the enthalpy, entropy, volume and heat capacity terms in Eq. 11 refer to properties of solid and molten J-garnet. Equation 11 can be simplified further by noting that (a) the ΔC_P^0 term can be neglected as it is much smaller than the other terms in Eq. 11 over wide temperature

ranges (Wood and Fraser 1976; Wood and Blundy 1997) (b) in the pressure range relevant to garnet-melt partitioning models, volumes of fusion are close to linear functions of pressure. These simplifications lead to

$$\begin{aligned} \Delta H_{f(0.1,T_f)}^0 - T \Delta S_{f(0.1,T_f)}^0 + P \Delta V + \frac{1}{2} \left(\frac{\partial \Delta V}{\partial P} \right) P^2 \\ = RT \ln \left(\frac{a_{J\text{-garnet}}^{\text{garnet}}}{a_{J\text{-garnet}}^{\text{melt}}} \right). \end{aligned} \quad (12)$$

The chemical composition and activity-composition relations of J-garnet can not be deduced by independent means. They are obtained through a trial-and-error procedure, using Eq. 12 to decide if assumptions are thermodynamically realistic. Because of the many variables involved, thermodynamically acceptable solutions are not necessarily unique. van Westrenen et al. (2001) assumed the J-garnet composition to be $\text{JMg}_2\text{Al}_3\text{Si}_2\text{O}_{12}$, a fictive REE-pyrope garnet incorporating J via a yttrium–aluminum garnet (YAG, $\text{Y}_3\text{Al}_5\text{O}_{12}$)-type charge-balancing mechanism. They also considered the simplest possible activity-composition models for J-garnet in both garnet and melt, and then used the 18 garnet-melt REE partitioning data sets available at the time to deduce the enthalpy, entropy, and volume of fusion of $\text{JMg}_2\text{Al}_3\text{Si}_2\text{O}_{12}$ through Eq. 12.

As mentioned above, this model fails to predict correctly both majorite-melt D 's (Draper et al. 2003, 2006; Dwarzski et al. 2006) and garnet-melt D 's at relatively low temperatures (e.g., Klemme et al. 2002; Bennett et al. 2004; Pertermann et al. 2004). The major extension in pressure, temperature, and bulk compositional range of the data available for this study allowed us to re-evaluate our previous choice of J-garnet component. This analysis strongly suggests that a fictive REE-almandine garnet component, $\text{JFe}_2\text{Al}_3\text{Si}_2\text{O}_{12}$, leads to a more accurate description of the thermodynamics of garnet-melt REE partitioning, both at high pressures, at low temperatures, and in iron-rich compositions relevant to the Moon and Mars (Draper et al. 2003, 2006).

Analogous to van Westrenen et al. (2001), we made simple assumptions about the activities of $\text{JFe}_2\text{Al}_3\text{Si}_2\text{O}_{12}$ in garnet and melt. Assuming complete ordering on the garnet Y and Z sites, and incorporating a measure of garnet non-ideality,

$$a_{\text{JFe}_2\text{Al}_3\text{Si}_2\text{O}_{12}}^{\text{garnet}} = \frac{27}{4} X_J^{\text{garnet}} (\gamma_{\text{Fe}}^{\text{garnet}} X_{\text{Fe}}^{\text{garnet}})^2 \quad (13)$$

where X_J^{garnet} is the mole fraction of J on the garnet X-site, $X_{\text{Fe}}^{\text{garnet}} = \text{Fe}^{2+}/(\text{Mg} + \text{Ca} + \text{Fe}^{2+} + \text{Mn})$. The factor 27/4 in Eq. 13 ensures that the activity of this component in a pure $\text{JFe}_2\text{Al}_3\text{Si}_2\text{O}_{12}$ system remains equal to unity. $\gamma_{\text{Fe}}^{\text{garnet}}$ is the activity coefficient for Fe in garnet, taking into account

the significant non-ideality along the almandine-grossular join (e.g., Geiger 1999):

$$\gamma_{\text{Fe}}^{\text{garnet}} = \exp\left(\frac{19000(X_{\text{Ca}}^{\text{garnet}})^2}{8.314T}\right) \quad (14)$$

where $X_{\text{Ca}}^{\text{garnet}} = \text{Ca}/(\text{Mg} + \text{Ca} + \text{Fe}^{2+} + \text{Mn})$ and T is in Kelvin.

For the melt, ideal mixing of $\text{JFe}_2\text{Al}_3\text{Si}_2\text{O}_{12}$ with other silicate melt components on a 12 oxygen basis was assumed, leading to

$$a_{\text{JFe}_2\text{Al}_3\text{Si}_2\text{O}_{12}}^{\text{melt}} = \frac{27}{4} X_{\text{J}}^{\text{melt}} (X_{\text{Fe}}^{\text{melt}})^2 \quad (15)$$

where $X_{\text{J}}^{\text{melt}}$ and $X_{\text{Fe}}^{\text{melt}}$ are the numbers of atoms of J and Fe^{2+} per 12 oxygens in the melt, respectively. Again, the factor 27/4 ensures that the activity of this component in a pure $\text{JFe}_2\text{Al}_3\text{Si}_2\text{O}_{12}$ system is one. Making these assumptions, Eq. 12 becomes

$$\begin{aligned} \Delta H_{f(0.1,T_f)}^0 - T\Delta S_{f(0.1,T_f)}^0 + P\Delta V + \frac{1}{2}\left(\frac{\partial\Delta V}{\partial P}\right)P^2 \\ = RT \ln\left(\left(\gamma_{\text{Fe}}^{\text{garnet}} D_{\text{Fe}}\right)^2 D_0(3+)\right). \end{aligned} \quad (16)$$

The molar fractions X used in Eqs. 13–15 have been converted to weight fractions (D values) in Eq. 16 making use of the fact that the mean molecular weights of garnets and melts (on a 12 oxygen basis) in anhydrous systems are within 2% relative of each other (van Westrenen et al. 2001). Equation 16 predicts a quantitative link between a thermodynamic description of the fusion of pure $\text{JFe}_2\text{Al}_3\text{Si}_2\text{O}_{12}$ and the distribution of REE between multi-component, natural garnets and melts. It constitutes a predictive model for D_0 , provided the enthalpy, entropy, and volume of fusion of pure $\text{JFe}_2\text{Al}_3\text{Si}_2\text{O}_{12}$ are known or accurately estimated. At present, no thermodynamic data are available for melting of REE-bearing alumino-silicate garnets. Below we show how $\Delta S_{f(0.1,T_f)}^0$, $\Delta H_{f(0.1,T_f)}^0$, and ΔV can in fact be accurately estimated using partitioning data. We then compare resulting estimates to known measurements of the thermodynamics of melting of end-member garnets.

Entropy of fusion

The entropy of fusion of $\text{JFe}_2\text{Al}_3\text{Si}_2\text{O}_{12}$, $\Delta S_{f(P,T_f)}^0$, can be estimated by analysing a set of partitioning experiments performed at constant pressure over a wide range of temperatures. In this case, the pressure terms in Eq. 16 are constant, and the right hand side of the equation can be calculated from measured values of garnet and melt major element composition, and fitted values of D_0 . $\Delta S_{f(P,T_f)}^0$ can

then be obtained from the slope of a plot of apparent free energy of fusion versus temperature.

As was the case in 2001, the anhydrous garnet-melt partitioning database is dominated by experiments performed at 3 ± 0.2 GPa ($n = 34$, Table 1). Twenty-five of these are iron-bearing, a requirement to be able to use Eq. 16. Calculated apparent free energies of fusion for $\text{JFe}_2\text{Al}_3\text{Si}_2\text{O}_{12}$ in these 3 GPa experiments are plotted against temperature in Fig. 7. The slope of the resulting straight line gives $\Delta S_{f(3\text{GPa},T_f)}^0 = 218 \pm 7 \text{ J mol}^{-1} \text{ K}^{-1}$. This value is similar to the best-fit value $226 \pm 23 \text{ J mol}^{-1} \text{ K}^{-1}$ previously derived for $\text{JMg}_2\text{Al}_3\text{Si}_2\text{O}_{12}$ (van Westrenen et al. 2001). The 1σ error of $7 \text{ J mol}^{-1} \text{ K}^{-1}$ derived from analysis of garnet-melt partitioning data approaches typical errors quoted for calorimetric entropy of fusion measurements for garnets (e.g., Newton et al. 1977; Téqui et al. 1991). The error is also significantly smaller than $1\sigma = 23 \text{ J mol}^{-1} \text{ K}^{-1}$ previously derived for $\text{JMg}_2\text{Al}_3\text{Si}_2\text{O}_{12}$, due to the much larger temperature range available (300 K compared to 150 K). The entropy of fusion is within error of an interpolation between calorimetric data for pure pyrope ($\Delta S_{f(0.1,T_f)}^0 = 162 \pm 5 \text{ J mol}^{-1} \text{ K}^{-1}$ —Newton et al. 1977; $\Delta S_{f(0.1,T_f)}^0 = 154 \text{ J mol}^{-1} \text{ K}^{-1}$ —Téqui et al. 1991) and YAG ($230 \text{ J mol}^{-1} \text{ K}^{-1}$ —Lin et al. 1999). Replacement of either Mg or Fe by trivalent cations, charge-balanced by replacing Si by Al, thus leads to an increase in the entropy of fusion of the resulting garnet component.

The effect of pressure on $\Delta S_{f(P,T_f)}^0$, calculated from average garnet thermal expansion data (Fei 1995) to be approximately $8 \text{ J mol}^{-1} \text{ K}^{-1}$ over the pressure range from

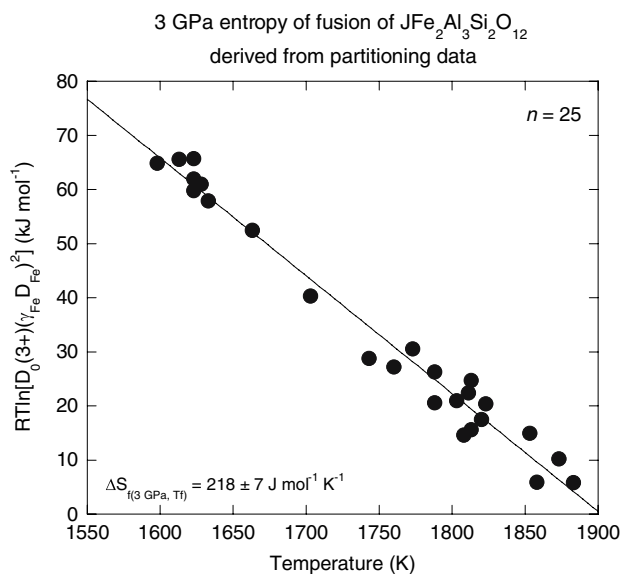


Fig. 7 The apparent free energy of fusion of $\text{JFe}_2\text{Al}_3\text{Si}_2\text{O}_{12}$ plotted against temperature, using 25 Fe-bearing experiments at 3 ± 0.2 GPa from Table 1. The entropy of fusion of $\text{JFe}_2\text{Al}_3\text{Si}_2\text{O}_{12}$ is derived from the slope of the straight line fitted through the data

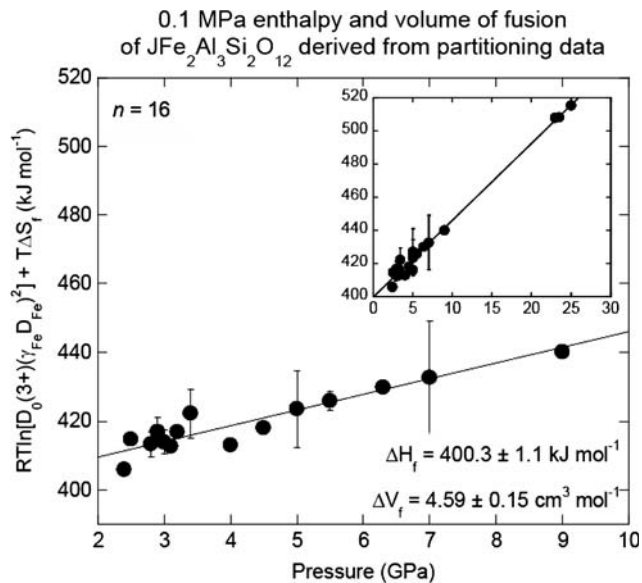


Fig. 8 The apparent free energy of fusion of $\text{JFe}_2\text{Al}_3\text{Si}_2\text{O}_{12}$, corrected for temperature using the entropy of fusion derived in Fig. 7, plotted against pressure (*symbols*, derived from garnet-melt REE partitioning data for experiments listed in Table 1). The enthalpy and volume of fusion of $\text{JFe}_2\text{Al}_3\text{Si}_2\text{O}_{12}$ are obtained from the intercept and slope, respectively, of a least-squares linear fit to the data between 2.4 and 9 GPa. The *inset* shows how the extrapolation of this ‘low-pressure’ fit (*line*) agrees very well with the 23–25 GPa data points

2.5 to 25 GPa, is similar to the 1σ error resulting from our fitting method ($7 \text{ J mol}^{-1} \text{ K}^{-1}$). Following van Westrenen et al. (2001) we therefore applied our value of $\Delta S_{f(3\text{GPa}, T_f)}^0$ to compensate for the temperature effect on *all* garnet-melt partitioning data irrespective of pressure. This allows us to estimate the enthalpy and volume of fusion for $\text{JFe}_2\text{Al}_3\text{Si}_2\text{O}_{12}$ using the partitioning data from Table 1. After rearranging Eq. 16, including our estimate for $\Delta S_{f(P, T_f)}^0$, we obtain:

$$\begin{aligned} RT \ln \left((\gamma_{\text{Fe}}^{\text{garnet}} D_{\text{Fe}})^2 D_0(3+) \right) + 218(\pm 7)T \\ = \Delta H_{f(0.1, T_f)}^0 + P\Delta V + \frac{1}{2} \left(\frac{\partial \Delta V}{\partial P} \right) P^2. \end{aligned} \quad (17)$$

Enthalpy and volume of fusion

By plotting the left hand side of Eq. 16 against pressure, information is obtained about $\Delta H_{f(0.1, T_f)}^0$ and $\Delta V_{f(0.1, T_f)}^0$ (Fig. 8). Experiments are now available at 19 different pressures between 2.4 and 25 GPa (Table 1), compared to four pressures in the van Westrenen et al. (2001) model. The pressure dependence in Fig. 8 appears to be linear rather than parabolic. In contrast to the model of Wood and Blundy (2002) we argue that the pressure derivative of the

volume change ($\frac{\partial \Delta V}{\partial P}$) in Eq. 17 is therefore negligible. We note that this conclusion could change once reliable majorite-melt partitioning data filling in the pressure gap between 9 and 23 GPa become available.

The pressure range for which garnet-melt partitioning data are now available is very large. As a result, inferences about pressure and temperature dependencies on garnet-melt D values, especially at the highest pressures, could be affected by inter-laboratory differences in pressure calibration. To prevent unwarranted propagation of possible pressure calibration errors, the slope and intercept of the best-fit line in Fig. 8 were derived from data obtained between 2.4 and 9 GPa only, leading to $\Delta H_{f(0.1, T_f)}^0 = 400.3 \pm 1.1 \text{ kJ mol}^{-1}$ and $\Delta V_{f(0.1, T_f)}^0 = 4.59 \pm 0.15 \text{ cm}^3 \text{ mol}^{-1}$. As seen in the inset of Fig. 8, these values are fully consistent with the 23–25 GPa data. We conclude that there are no systematic errors in pressure calibration between the lower and higher pressure data sets in Table 1.

The enthalpy of fusion of $\text{JFe}_2\text{Al}_3\text{Si}_2\text{O}_{12}$ is similar to the value of $418 \pm 12 \text{ kJ mol}^{-1}$ previously obtained for $\text{JMg}_2\text{Al}_3\text{Si}_2\text{O}_{12}$ by van Westrenen et al. (2001). However, the volume of fusion of $\text{JFe}_2\text{Al}_3\text{Si}_2\text{O}_{12}$ is less than half the value of $\Delta V_{f(0.1, T_f)}^0 = 10.4 \pm 1.0 \text{ cm}^3 \text{ mol}^{-1}$ derived for $\text{JMg}_2\text{Al}_3\text{Si}_2\text{O}_{12}$. Again, errors in the thermodynamic fusion properties of $\text{JFe}_2\text{Al}_3\text{Si}_2\text{O}_{12}$ are significantly reduced because of the growth of the data set covering a much wider pressure range. Calorimetric data on YAG (Lin et al. 1999) show that YAG has an estimated $\Delta H_{f(0.1, T_f)}^0$ of 516 kJ mol^{-1} . Our derived value of $400.3 \pm 1.1 \text{ kJ mol}^{-1}$ is therefore what might be expected from a progression from pyrope to YAG. The estimated melting point of $\text{JFe}_2\text{Al}_3\text{Si}_2\text{O}_{12}$ is $1,835 \pm 60 \text{ K}$, slightly lower than that of $\text{JMg}_2\text{Al}_3\text{Si}_2\text{O}_{12}$ ($T_f = 1,850 \pm 140 \text{ K}$, van Westrenen et al. 2001), in accordance with an observed decrease in melting temperature going from pyrope to almandine (Butvina et al. 2001). T_f is in between the known values for pyrope ($1,570 \pm 30 \text{ K}$, van Westrenen et al. 2001) and YAG ($1,970 \pm 30 \text{ K}$, Fratello and Brandle 1993).

Predicting D_0

In summary, the entropy of fusion of hypothetical REE garnet compound $\text{JFe}_2\text{Al}_3\text{Si}_2\text{O}_{12}$, derived from garnet-melt REE partitioning data, is $218 \pm 7 \text{ J mol}^{-1} \text{ K}^{-1}$, its enthalpy of fusion is $400.3 \pm 1.1 \text{ kJ mol}^{-1}$, and its volume of fusion is $4.59 \pm 0.15 \text{ cm}^3 \text{ mol}^{-1}$. These values can be used to predict D_0 , using Eq. 17 (where R is the gas constant, T in Kelvin, P in GPa, and $\gamma_{\text{Fe}}^{\text{garnet}}$ is taken from Eq. 14), to yield

$$\begin{aligned} D_0(\text{REE}) \\ = \exp \left(\frac{400290(\pm 1100) + 4586(\pm 150)P - 218(\pm 7)T}{RT} \right) / (\gamma_{\text{Fe}}^{\text{garnet}} D_{\text{Fe}})^2. \end{aligned} \quad (18)$$

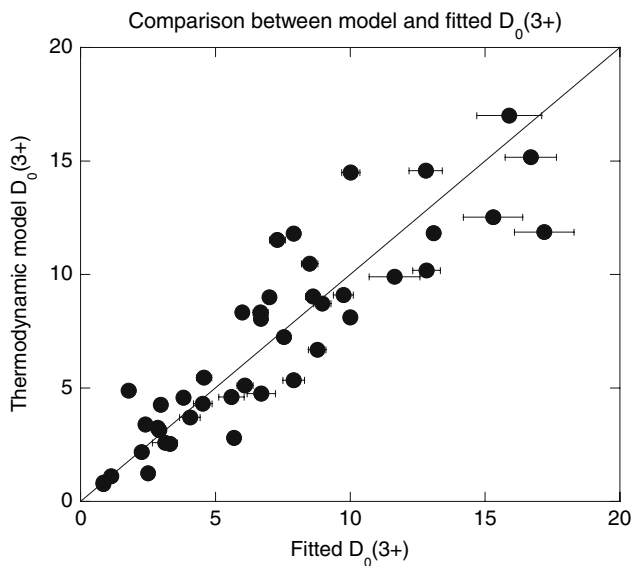


Fig. 9 Comparison between fitted D_0 and thermodynamically predicted D_0 (Eq. 18) for experiments listed in Table 1

Equation 18 does not incorporate any explicit term to deal with effects on D_0 of increasing Si (as pressure increases) or increasing Ti concentrations in the garnet Y-site. Si and Ti on the garnet Y-site to a first degree do not appear to influence the thermodynamics of REE exchange between garnet and melt. Eq. 18 does not take into account the possible influence of melt structure and/or composition on garnet-melt partitioning, apart from incorporating an explicit dependence on the Fe content of the melt through the D_{Fe} term. Whether melt composition and/or structure are important variables in mineral-melt partitioning continues to be hotly debated (e.g., Blundy and Wood 2003a; Gaetani 2004; Schmidt et al. 2006). In the companion paper (Draper and van Westrenen this issue) we will show that an alternative, statistical parameterisation of D_0 variations requires incorporation of an additional term involving Fe–Mg exchange between garnet and coexisting melt. Both D_0 models reproduce experimental data equally well. We conclude that the currently available garnet-melt partitioning data base cannot be used to argue either for or

Fig. 10 Comparison between measurements (symbols) and predictions using the models for r_0 , E , and D_0 presented in this study (solid curves, constructed by combining Eqs. 1, 3, 6, and 18). Data are shown for a representative low-pressure, low-temperature garnet (a, from Salters et al. 2002), and representative majorite-poor and majorite-rich garnets at high P and T (b, from Dwarzski et al. 2006 and c, from Tuff and Gibson 2007). Dotted curves in c illustrate how predicted values vary if experimental charges were at temperatures 25 K lower (upper curve) or higher (lower curve) than indicated by the thermocouple junction

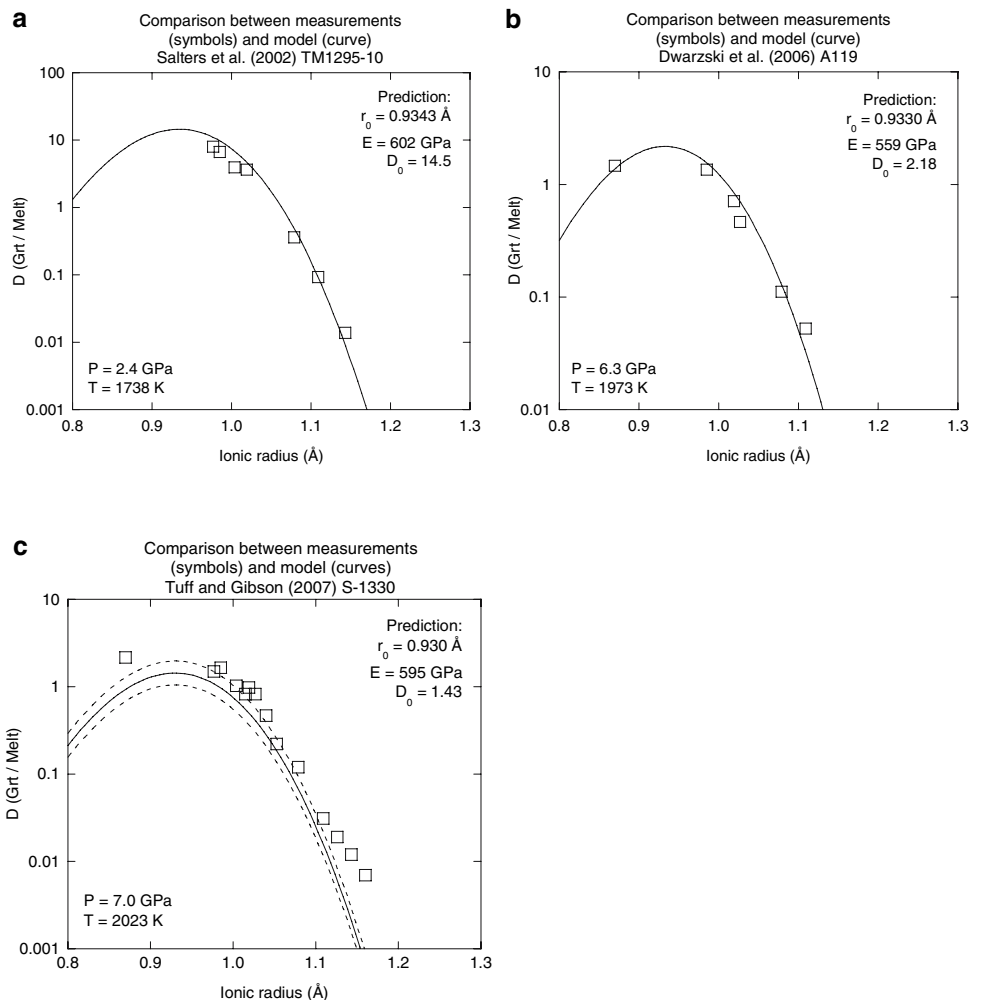


Table 2 Mismatches (in per cent) between measured and predicted values of garnet-melt partition coefficients from Table 1

Mismatch (per cent)	Ce	Nd	Sm	Eu	Gd	Dy	Er	Yb	Lu	Y	Sc
Minimum	25	10	0.2	3.0	2.1	5.0	1.7	0.0	2.2	1.0	0.8
Maximum	96	127	103	117	61	218	73	160	74	147	131
Average	70	53	42	37	26	50	25	37.1	33	38	33

against a melt compositional effect on garnet-melt D values.

A comparison between predicted and fitted D_0 values for the REE, Y and Sc for the experiments from Table 1 is shown in Fig. 9. D_0 values varying by over one order or magnitude can be predicted with confidence across the P – T range of garnet stability, including pressures of 25 GPa.

Together, Eqs. 1, 3, 6 and 18 can be used to predict $D_{\text{REE,Y,Sc}}$ as a function of pressure, temperature, garnet major element composition, and D_{Fe} . Three examples of this are shown in Fig. 10. Figure 10c shows a comparison between our predictive model and a recently published dataset (Tuff and Gibson 2007) which was not used for any aspect of model construction. To highlight the sensitivity of our model to temperature variations, dotted curves in Fig. 10c illustrate how model predictions vary if temperature is raised or lowered by 25 K compared to the experimental run temperature quoted in Tuff and Gibson (2007). Errors in experimental temperatures on the order of ± 25 K are common at the high temperatures required to equilibrate garnet and melt at pressures >3 GPa, and this could well be a reason for some of the relatively small remaining discrepancies between model and data.

Table 2 lists standard deviations of the difference between predicted and observed $D_{\text{REE,Y,Sc}}$ (total $n > 300$) that stem from the propagation of errors in the prediction of the three individual lattice-strain parameters. These deviations average from 25% for Er to 70% for Ce. The maximum error in D prediction is 218% for one measurement of D_{Dy} . This is remarkably low considering the total spread in $D_{\text{REE,Y,Sc}}$ values of over four orders of magnitude.

Conclusion

Accurate prediction of garnet-anhydrous melt and majorite-anhydrous melt D 's for the REE, Y and Sc is possible with a single thermodynamic, lattice-strain based model. Our calibration is capable of predicting D 's to use in modelling of partial melting processes at pressures covering the entire stability range of magmatic garnets in the Earth, Moon and Mars.

Acknowledgments This work was funded by US NSF grant EAR-0337237 to DSD and a European Young Investigator (EURYI) award to WvW. Comments by Marc Hirschmann, Yakov Khazan, and an

anonymous reviewer greatly improved the clarity of this manuscript. We thank Lee Ann Lloyd, Janice Noruk, Rama Murthy, and the Community of Corrales, NM for fantastic logistical support. Surprising input by S. I. van Westrenen is gratefully acknowledged.

References

- Allègre CJ, Minster JF (1978) Quantitative models of trace element behavior in magmatic processes. *Earth Planet Sci Lett* 38:1–25
- Anderson OL (1972) Patterns in elastic constants of minerals important to geophysics. In: Robertson EC (ed) *The nature of the solid earth*. McGraw-Hill, New York, pp 575–613
- Beattie P (1994) Systematics and energetics of trace-element partitioning between olivine and silicate melts: implications for the nature of mineral/melt partitioning. *Chem Geol* 117:57–71
- Beattie P, Drake M, Jones J, Leeman W, Longhi J, McKay G, Nielsen R, Palme H, Shaw D, Takahashi E, Watson B (1993) Terminology for trace-element partitioning. *Geochim Cosmochim Acta* 57:1605–1606
- Bennett SL, Blundy J, Elliott T (2004) The effect of sodium and titanium on crystal-melt partitioning of trace elements. *Geochim Cosmochim Acta* 68:2335–2347
- Blundy JD, Wood BJ (1994) Prediction of crystal-melt partition coefficients from elastic moduli. *Nature* 372:452–454
- Blundy JD, Wood BJ (2003a) Partitioning of trace elements between crystals and melts. *Earth Planet Sci Lett* 210:383–397
- Blundy JD, Wood BJ (2003b) Mineral-melt partitioning of uranium, thorium and their daughters. *Rev Miner Geochem* 52:39–123
- Blundy JD, Falloon TJ, Wood BJ, Dalton JA (1995) Sodium partitioning between clinopyroxene and silicate melts. *J Geophys Res* 100:15501–15515
- Borg LE, Draper DS (2003) A petrogenetic model for the origin and compositional variation of the martian basaltic meteorites. *Meteor Planet Sci* 38:1713–1731
- Brice JC (1975) Some thermodynamic aspects of the growth of strained crystals. *J Crystal Growth* 28:249–253
- Butvina VG, Bobrov AV, Litvin YA (2001) Experimental study of the pyrope-grossular-almandine system at 6.5 GPa and 1500–1900°C. *Doklady Akademii nauk* 379:655–658 (in Russian)
- Corgne A, Wood BJ (2004) Trace element partitioning between majoritic garnet and silicate melt at 25 GPa. *Phys Earth Planet Int* 143–144:407–419
- Drake MJ, McFarlane EA, Gasparik T, Rubie DC (1993) Mg-perovskite/silicate melt and majorite garnet/silicate melt partition coefficients in the system CaO–MgO–SiO₂ at high temperatures and pressures. *J Geophys Res* 98:5427–5431
- Draper DS, Xirouchakis D, Agee CB (2003) Trace element partitioning between garnet and chondritic melt from 5 to 9 GPa: implications for the onset of the majorite transition in the martian mantle. *Phys Earth Planet Int* 139:149–169
- Draper DS, duFrane SA, Shearer CK, Dwarzski RE, Agee CB (2006) High-pressure phase equilibria and element partitioning experiments on Apollo 15 green C picritic glass: implications for the role of garnet in the deep lunar interior. *Geochim Cosmochim Acta* 70:2400–2416

- Dwarzski RE, Draper DS, Shearer CK, Agee CB (2006) Preliminary insights on the crystal chemistry of high titanium garnets from partitioning of rare earth and high field strength elements. *Am Mineral* 91:1536–1546
- Fei Y (1995) Thermal expansion. In: Mineral physics and crystallography. A handbook of physical constants. AGU reference shelf 2, pp 29–44
- Fratello VJ, Brandle CD (1993) Physical properties of a $Y_3Al_5O_{12}$ melt. *J Crystal Growth* 128:1006–1010
- Gaetani GA (2004) The influence of melt structure on trace element partitioning near the peridotite solidus. *Contrib Mineral Petrol* 147:511–527
- Gast PW (1968) Trace element fractionation and the origin of tholeiitic and alkaline magma types. *Geochim Cosmochim Acta* 32:1057–1086
- Geiger CA (1999) Thermodynamics of $(Fe^{2+}, Mn^{2+}, Mg, Ca)_3Al_2Si_3O_{12}$ garnet: a review and analysis. *Mineral Petrol* 66:271–299
- Gibbs GV, Smith JV (1965) Refinement of the crystal structure of synthetic pyrope. *Am Mineral* 50:2032–2039
- Goldschmidt VM (1937) The principles of distribution of chemical elements in minerals and rocks. *J Chem Soc* 655:655–673
- Hanchar JM, van Westrenen W (2007) Rare earth element behavior in zircon/melt systems. *Elements* 3:37–42
- Hauri EH, Wagner TP, Grove TL (1994) Experimental and natural partitioning of Th, U, Pb and other trace elements between garnet, clinopyroxene and basaltic melts. *Chem Geol* 117:149–166
- Hazen RM, Finger LW (1979) Bulk modulus-volume relationship for cation–anion polyhedra. *J Geophys Res* 84:6723–6728
- Hellebrand E, Snow JE, Hoppe P, Hofmann AW (2002) Garnet-field melting and late-stage refertilization in ‘residual’ abyssal peridotites from the Central Indian ridge. *J Petrol* 43:2305–2338
- Hertogen J, Gijbels R (1976) Calculation of trace element fractionation during partial melting. *Geochim Cosmochim Acta* 40:313–322
- Hill E, Wood BJ, Blundy JD (2000) The effect of Ca-Tschemmacks component on trace element partitioning between clinopyroxene and silicate melt. *Lithos* 53:203–215
- Johnson KTM (1998) Experimental determination of partition coefficients for rare earth and high-field-strength elements between clinopyroxene, garnet, and basaltic melt at high pressures. *Contrib Mineral Petrol* 133:60–68
- Kato T, Ringwood AE, Irifune T (1988) Experimental determination of element partitioning between silicate perovskites, garnets and liquids: constraints on early differentiation of the mantle. *Earth Planet Sci Lett* 89:123–145
- Klemme S, Blundy JD, Wood BJ (2002) Experimental constraints on major and trace element partitioning during partial melting of eclogite. *Geochim Cosmochim Acta* 66:3109–3123
- Lin I-C, Navrotsky A, Weber JKR, Nordine PC (1999) Thermodynamics of glass formation and metastable solidification of molten $Y_3Al_5O_{12}$. *J Non-Cryst Sol* 243:273–276
- Merli M, Callegari A, Cannillo E, Caucia F, Leona M, Oberti R, Ungaretti L (1995) Crystal-chemical complexity in natural garnets: structural constraints on chemical variability. *Eur J Mineral* 7:1239–1249
- Moriyama J, Kawabe I, Fujino K, Ohtani E (1992) Experimental study of element partitioning between majorite, olivine, merwinite, diopside and silicate melts at 16 GPa and 2000°C. *Geochem J* 26:357–382
- Mysen BO (2004) Element partitioning between minerals and melt, melt composition, and melt structure. *Chem Geol* 213:1–24
- Nagasawa H (1966) Trace element partition coefficient in ionic crystals. *Science* 152:767–769
- Neal CR (2001) Interior of the Moon: the presence of garnet in the primitive deep lunar mantle. *J Geophys Res* 106:27865–27885
- Neumann H, Mead J, Vitaliano CJ (1954) Trace element variation during fractional crystallization as calculated from the distribution law. *Geochim Cosmochim Acta* 6:90–99
- Newton RC, Charlu TV, Kleppa OJ (1977) Thermochemistry of high pressure garnets and clinopyroxenes in the system $CaO-MgO-Al_2O_3-SiO_2$. *Geochim Cosmochim Acta* 41:369–377
- Ohtani E, Kawabe I, Moriyama J, Nagata Y (1989) Partitioning of elements between majorite garnet and melt and implications for petrogenesis of komatiite. *Contrib Mineral Petrol* 103:263–269
- Onuma N, Higuchi H, Wakita H, Nagasawa H (1968) Trace element partition between two pyroxenes and the host lava. *Earth Planet Sci Lett* 5:47–51
- Pertermann M, Hirschmann MM, Hametner K, Günther D, Schmidt MW (2004) Experimental determination of trace element partitioning between garnet and silica-rich liquid during anhydrous partial melting of MORB-like eclogite. *Geochem Geophys Geosys* 5. doi: 10.1029/2003GC000638
- Press WH, Teukolsky SA, Vetterling WT, Flannery BP (1992) Numerical recipes in C. Cambridge University Press, Cambridge, p 965
- Prowatke S, Klemme S (2005) Effect of melt composition on the partitioning of trace elements between titanite and silicate melt. *Geochim Cosmochim Acta* 69:695–709
- Quartieri S, Antonioli G, Geiger CA, Artioli G, Lottici PP (1999a) XAFS characterization of the structural site of Yb in synthetic pyrope and grossular garnets. *Phys Chem Minerals* 26:251–256
- Quartieri S, Chaboy J, Antonioli G, Geiger CA (1999b) XAFS characterization of the structural site of Yb in synthetic pyrope and grossular garnets. II: XANES full multiple scattering calculations at the Yb L_I- and L_{III} edges. *Phys Chem Minerals* 27:88–94
- Quartieri S, Boscherini F, Chaboy J, Dalconi MC, Oberti R, Zanetti A (2002) Characterization of trace Nd and Ce site preference and coordination in natural melaniets: a combined X-ray diffraction and high-energy XAFS study. *Phys Chem Minerals* 29:495–502
- Quartieri S, Dalconi MC, Boscherini F, Oberti R, D’Acapito F (2004) Changes in the local coordination of trace rare-earth elements in garnets by high-energy XAFS: new data on dysprosium. *Phys Chem Minerals* 31:162–167
- Salters VJM, Hart SR (1989) The hafnium paradox and the role of garnet in the source of mid-ocean-ridge basalts. *Nature* 342:420–422
- Salters VJM, Longhi J (1999) Trace element partitioning during the initial stages of melting beneath mid-ocean ridges. *Earth Planet Sci Lett* 166:15–30
- Salters VJM, Longhi JE, Bizimis M (2002) Near mantle solidus trace element partitioning at pressures up to 3.4 GPa. *Geochem Geophys Geosys* 3. doi: 10.1029/2001GC000148
- Schmidt MW, Connolly JAD, Günther D, Bogaerts M (2006) Element partitioning: the role of melt structure and composition. *Science* 312:1646–1650
- Shaw DM (1953) The camouflage principle and trace-element distribution in magmatic minerals. *J Geol* 61:142–151
- Shaw DM (1970) Trace element fractionation during anatexis. *Geochim Cosmochim Acta* 34:237–243
- Shen Y, Forsyth DW (1995) Geochemical constraints on the initial and final depth of melting beneath mid-ocean ridges. *J Geophys Res* 100:2211–2237
- Téqui C, Robie RA, Hemingway BS, Neuville DR, Richet P (1991) Melting and thermodynamic properties of pyrope ($Mg_3Al_2Si_3O_{12}$). *Geochim Cosmochim Acta* 55:1005–1010
- Tuff J, Gibson SA (2007) Trace-element partitioning between garnet, clinopyroxene and Fe-rich picritic melts at 3 to 7 GPa. *Contrib Mineral Petrol* 153:369–387

- Ungaretti L, Leona M, Merli M, Oberti R (1995) Non-ideal solid-solution in garnet: crystal-structure evidence and modelling. *Eur J Mineral* 7:1299–1312
- Walter MJ, Nakamura E, Trønnes RG, Frost DJ (2004) Experimental constraints on crystallization differentiation in a deep magma ocean. *Geochim Cosmochim Acta* 68:4267–4284
- van Westrenen W, Blundy JD, Wood BJ (1999) Crystal-chemical controls on trace element partitioning between garnet and anhydrous silicate melt. *Am Mineral* 84:838–847
- van Westrenen W, Blundy JD, Wood BJ (2000a) Effect of Fe^{2+} on garnet-melt trace element partitioning: experiments in FCMAS and quantification of crystal-chemical controls in natural systems. *Lithos* 53:191–203
- van Westrenen W, Allan NL, Blundy JD, Purton JA, Wood BJ (2000b) Atomistic simulation of trace element incorporation into garnets—comparison with experimental garnet-melt partitioning data. *Geochim Cosmochim Acta* 64:1629–1639
- van Westrenen W, Wood BJ, Blundy JD (2001) A predictive thermodynamic model of garnet-melt trace element partitioning. *Contrib Mineral Petrol* 142:219–234
- Whitney DL, Broz M, Cook RF (2007) Hardness, toughness, and modulus of some common metamorphic minerals. *Am Mineral* 92:281–288
- Withers AC (1997) Water in the mantle. Ph.D. thesis, University of Bristol, UK, p 195
- Wood BJ, Blundy JD (1997) A predictive model for rare earth element partitioning between clinopyroxene and anhydrous silicate melt. *Contrib Mineral Petrol* 129:166–181
- Wood BJ, Blundy JD (2001) The effect of cation charge on crystal-melt partitioning. *Earth Planet Sci Lett* 188:59–71
- Wood BJ, Blundy JD (2002) The effect of H_2O on crystal-melt partitioning of trace elements. *Geochim Cosmochim Acta* 66:3647–3656
- Wood BJ, Fraser DG (1976) Elementary thermodynamics for geologists. Oxford University Press, Oxford, 303 p
- Yurimoto H, Ohtani E (1992) Element partitioning between majorite and liquid: a secondary ion mass spectrometric study. *Geophys Res Lett* 19:17–20
- Zhang L, Ahsbabs H, Kutoglu A (1998) Hydrostatic compression and crystal structure of pyrope up to 33 GPa. *Phys Chem Minerals* 25:301–307
- Zou H, Reid MR (2001) Quantitative modeling of trace element fractionation during incongruent dynamic melting. *Geochim Cosmochim Acta* 65:153–162